Effects of Jet Impingement on Convective Heat Transfer in Effusion Holes

Nathan C. Huelsmann
Department of Mechanical Engineering,
Pennsylvania State University,
3127 Research Drive,
State College, PA 16801
e-mail: nuh98@psu.edu

Karen A. Thole
Mem. ASME
Department of Mechanical Engineering,
Pennsylvania State University,
136 Reber Building,
University Park, PA 16802
e-mails: kthole@engr.psu.edu;
kthole@psu.edu

A common design for cooling the combustor liner of gas turbines is a double wall composed of impingement jets that feed effusion cooling holes. An important cooling mechanism associated with the effusion hole is the convective cooling provided to the liner wall, which is in contact with the hot main gas flowing through the combustor. While the combination of impingement jets and effusion holes has been studied earlier, mostly in terms of cooling effectiveness, investigators have not fully evaluated the effect the impingement jet has on the local internal convection within the effusion hole. This study evaluates the detailed effects of the impingement geometry on the local convective heat transfer coefficients within the effusion hole, which provides insights as to the design decisions for cooling combustor liners. Using a scaled-up, 3D-printed effusion hole with a constant heat flux boundary condition, local convective heat transfer coefficients were measured for a range of impingement geometries and positions relative to the effusion holes. Results showed a strong influence on the convective heat transfer resulting from the placement of the impingement hole relative to the effusion hole. In particular, the results showed a strong sensitivity to the circumferential and radial placement of the impingement jet with little sensitivity to the jet-to-effusion distance. [DOI: 10.1115/1.4050335]

Introduction

Resulting from increased temperatures seen in modern combustors, effective cooling is necessary to ensure combustor liner durability. Current combustor liners are highly engineered with a double-wall design containing impingement and effusion cooling. Impingement jets cool the backside wall, while effusion jets create a protective film over the external wall. Internal convection from the effusion holes has also been shown to play a large role in the overall cooling of the combustor liner walls. What is not known is how the coolant feed from the impingement hole that supplies the effusion hole affects the internal convective cooling from the effusion hole, especially at the entrance region of the effusion hole. In many designs, the impingement hole location relative to the effusion hole entrance can vary, whether it be from manufacturing tolerances or design constraints. This variation can, in fact, affect the internal convection from the effusion holes leading to either better cooling or detrimental temperatures.

In the existing literature, numerous studies have reported adiabatic effectiveness and overall effectiveness for double-wall combustor liners [1–4]. However, few studies have reported the details of internal convection within effusion holes that are supplied by impingement jets. The uniqueness of this article is that numerous experiments were conducted in which the local and averaged internal convection coefficients of an effusion hole were measured for a wide variety of impingement jet locations. Given that the entrance conditions for the effusion jets can vary widely and the entrance flow is highly influential on the convective heat transfer, the focus of this study was on the entrance region of the effusion hole.

Literature Review

Only a few studies have been published on the internal heat transfer within film-cooling holes. Boelter et al. [5] studied the heat transfer in the entrance region of long circular tubes with varying entrance conditions such as angled bends or flared openings. This article showed high heat transfer at the entrance to the pipe in which he developed correlations to predict average heat transfer coefficients for the long pipes that were significantly longer than most film-cooling holes. In a study modeling, a combustor wall using the naphthalene sublimation method, Cho et al. [6] found local and average mass transfer coefficients through a circular, short hole ($L/D < 1.5$). They showed that a separation region was present at the hole entrance that decreased with the increasing Reynolds numbers until $Re > 5000$. It was also found that around 60% of the total mass transfer of the combustor liner was due to the convective heat transfer from the cooling holes. Kohli and Thole [7] performed a computational fluid dynamics (CFD) analysis on angled film-cooling holes that showed a similar separation region at the inlet to the film-cooling holes that was very sensitive to the coolant supply direction.

An analytical model of film-cooling holes in a combustor wall by Martiny et al. [8] presented a method for optimization of cooling hole distributions. Similar to the study by Cho et al. [6], they found that 60% of the heat transfer was due to the internal heat transfer in the effusion holes. This assertion was further verified by Terrell et al. [9] through a combination of experimental and CFD results from film-cooling holes in a leading edge of a model turbine blade. They found that the coolant hole internal heat transfer accounted for 50–80% of the convective heat transfer.

Recently, Bryant and Rutledge [10] devised CFD models to isolate the cooling mechanisms present in the overall effectiveness of a single-wall external film-cooling design by varying boundary conditions. To evaluate the effect of internal hole cooling on the overall effectiveness, surfaces of the film-cooling hole were set to be adiabatic to remove the effect of internal cooling, and the results were then compared to the baseline case. In Bryant and Rutledge's results, internal hole cooling was most effective at cooling the upstream surface of the effusion hole and near the exit of the hole.

None of the previously discussed studies have evaluated internal convective cooling of effusion holes in relation to impingement positions, especially with respect to local measurements. To begin to close this knowledge gap, the current study adds data on the

Contributed by the International Gas Turbine Institute (IGTI) of ASME for publication in the Journal of Turbomachinery. Manuscript received September 24, 2020; final manuscript received January 2, 2021; published online April 8, 2021. Assoc. Editor: David G. Bogard.

Table 1 Effusion and impingement variables

	Impingement	Effusion
α (deg)	90	30
t_i/D	1	N/A
t_e/D	N/A	1.5, 3
H/D	3, 6	N/A
L/D	N/A	3, 6
r/D	0, 1, 3	N/A
θ (deg)	0, 90, 180, 270	N/A
Φ (deg)	N/A	−180, −135, −90, −45, 0, 45, 90, 135, 180

local heat transfer within the effusion hole as affected by varying impingement patterns.

Impingement and Effusion Geometries

A scaled-up, double-wall combustor liner with a single effusion hole and single impingement hole was constructed with the details given in Table 1 and shown in Fig. 1. Note that the entrance effects were the primary interest for this study and, as such, the exit crossflow was not simulated for the effusion hole since it does not have significant effects on the internal heat transfer as shown by Cho and Goldstein [11].

Both the effusion and impingement holes had the same diameter, D (2.54 cm) as shown in Fig. 1. The effusion hole was constructed as a single pipe that was 3D printed from a low thermal conductivity plastic. The printed effusion hole (pipe) allowed for specific thermocouple placement along the length of the pipe as well as around the circumference. Three different impingement plates containing a single hole were constructed, which allowed for testing at a multitude of positions, both radially as well as circumferentially, relative to the effusion hole. The impingement plate thickness, t_i, and impingement and effusion hole diameters, D, remained the same for each of the plates.

The impingement hole positions were varied between three radial positions, $r/D = 0$ (direct impingement), 1, and 3, as illustrated in Figs. 1 and 2. The impingement and effusion double-walled geometry combinations were created by switching out the impingement plate and by changing the impingement plate circumferential position by 90 deg intervals. Two jet-to-target spacing values were chosen for testing, $H/D = 3$ and 6, which are displayed in Fig. 1. In total, 19 different geometry combinations were tested.

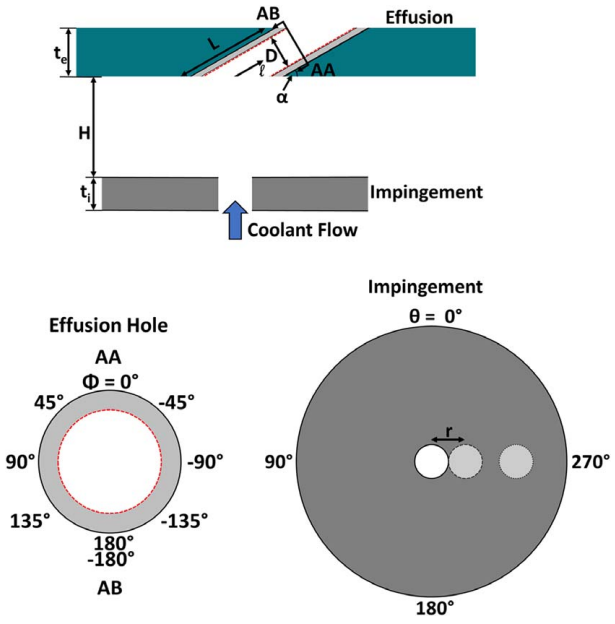

Fig. 1 Effusion hole and impingement hole geometries. Flow is exiting the page for the bottom models.

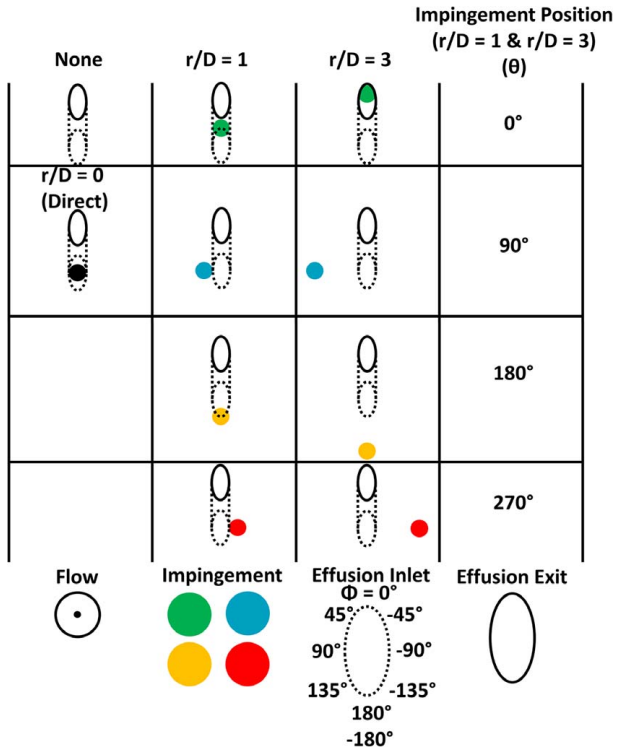

Fig. 2 Impingement and effusion geometries studied

Experimental Setup and Methods

To perform the heat transfer experiments, compressed air flowed through a sealed test rig containing the scaled-up impingement and effusion plates as shown in Fig. 3. The impingement plate was mounted inside of a larger pipe with two endcaps placed over either side of the pipe. The test rig with 8 effusion hole diameters avoids any sidewall effects. A foam insulation block surrounded the effusion hole to reduce heat losses during testing. The endcap upstream of the impingement plate included a nozzle and splash plate to diffuse the air flow entering the rig. The air flow was controlled using a mass flow controller.

Thermocouples were inserted into 38 slots located along the length and around the circumference of the effusion hole, so that the thermocouple beads were flush with the inner surface of the effusion hole as shown in Fig. 4. Each slot was then filled with a thermally conductive epoxy to ensure that the bead was in contact with the inner heat flux surface. Thermocouple placement started at the entrance to the pipe (effusion hole) and continued at every 10% interval along L/D up to $\ell/D = 2.7$.

A constant heat flux boundary condition was applied to the pipe walls of the effusion hole. The heater was made by adhering 16 stainless steel strips, each 0.0254 mm thick and 2.54 mm wide, between two Kapton sheets. The Kapton steel strip sandwich was then glued to the inner surface of the effusion hole with double-sided, high temperature adhesive. Thermocouples were attached to the backside of the heater sandwich to measure the local surface temperatures. For a given experiment, a constant power was input to the heater, and a Reynolds number at the effusion hole was set based on the mass flowrate of air measured and controlled by the mass flow controller. The static pressure and the flow temperature were measured at the inlet of the effusion hole. Reynolds numbers were varied between $2000 < Re < 11{,}000$.

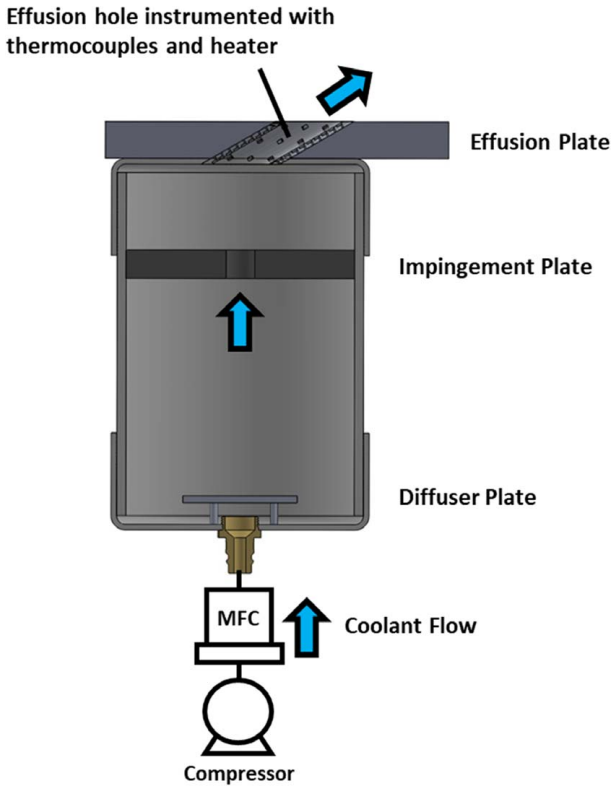

Fig. 3 Test facility showing impingement and effusion test plates

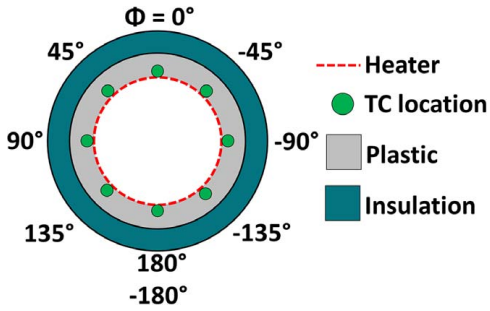

Fig. 4 Effusion hole instrumentation showing the heated surface with thermocouples placed radially around the effusion hole. Flow is exiting the page.

The heater power and surface temperatures were measured once the steady state was reached, which typically required ~3 h. The heat loss was accounted for by using thermocouples placed inside the insulating foam around the effusion hole and performing a conduction analysis. Conductive heat losses stayed within 2%–4% for all tests. After the heat loss was subtracted from the input power, local heat transfer coefficients were calculated based on the local mean temperature of the fluid, which was calculated using the first law analysis. The local heat transfer coefficient, h, for each position was calculated using Eq. (1), where the air temperature T_{air} was the local mean temperature and T_w was the wall surface temperature.

$$h = \frac{q''}{T_w - T_{air}} \tag{1}$$

An area-averaged heat transfer coefficient $\bar{\bar{h}}$ was found through an area-weighted formula shown in Eq. (2).

$$\bar{\bar{h}} = \frac{\sum h \cdot A}{A_{total}} \tag{2}$$

Experimental Uncertainty

Uncertainty in the experiments was calculated using the methods from Kline and McClintock [12]. The uncertainty of the local Nusselt numbers was found to be between 3% and 7% with uncertainty decreasing as the hole length increased and increasing as the Reynolds number increased. This increase in uncertainty is attributed to the smaller temperature difference between the cooling flow and the effusion wall temperature. Uncertainty for the averaged Nusselt numbers was found to be under 1% for all cases. Finally, uncertainty in the Reynolds number was found to be less than 1% for all cases.

Effect of Angular Impingement Location

As stated in the literature review, Kohli and Thole's [7] computational studies showed the influence that the coolant supply direction had on the film-cooling performance as well as the flow field within the cooling hole. Figures 5 and 6 show the area-averaged Nusselt numbers for the short and long effusion holes ($L/D = 3$ and 6) over the range of Reynolds numbers for differing jet impingement locations for the closest radial position, $r/D = 1$, and closest impingement distance, $H/D = 3$. Also shown in Figs. 5 and 6 is what would be expected from a fully developed pipe flow, as indicated by the Gnielinski correlation [13], as well as the measured convective heat transfer coefficients for direct jet impingement and no impingement cases.

For both effusion hole lengths, shown in Figs. 5 and 6, there is a substantially higher Nusselt number for all the cases relative to the fully developed pipe flow correlations, which indicates the benefit of the entry region on the convective cooling of the combustor liner. For the shorter effusion hole, $L/D = 3$, at a Re = 8000, there is a 148% higher Nusselt number for the no impingement case relative to the fully developed correlation. At the same Re = 8000 for the longer effusion hole, there is only a 104% higher Nusselt number for the no impingement case relative to the fully developed correlation. As the effusion hole increases in the length with more surface area, the benefits of the high heat transfer coefficients in the entry region are reduced.

Although it might be expected that direct impingement would result in the highest Nusselt numbers, the data in Figs. 5 and 6 indicate otherwise. In fact, the direct impingement is between the side injection (90 deg and 270 deg) cases and the in-line injection (0 deg and 180 deg). These results indicate a major flowfield change when feeding the effusion hole using side injection.

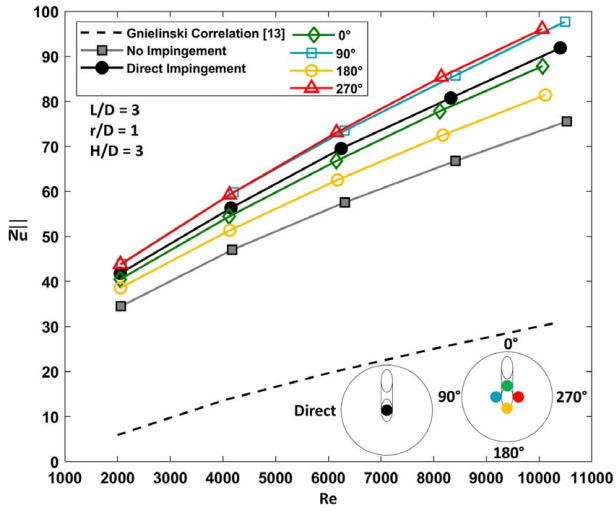

Fig. 5 Area-averaged Nusselt number for the short effusion hole, $L/D = 3$, with constant radial spacing, $r/D = 1$, and constant jet-to-target spacing, $H/D = 3$

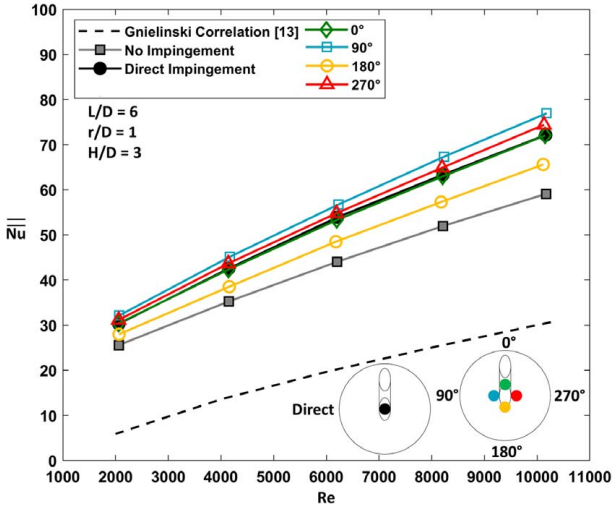

Fig. 6 Area-averaged Nusselt number for the long effusion hole, *L/D* = 6, with constant radial spacing, *r/D* = 1, and constant jet-to-target spacing, *H/D* = 3

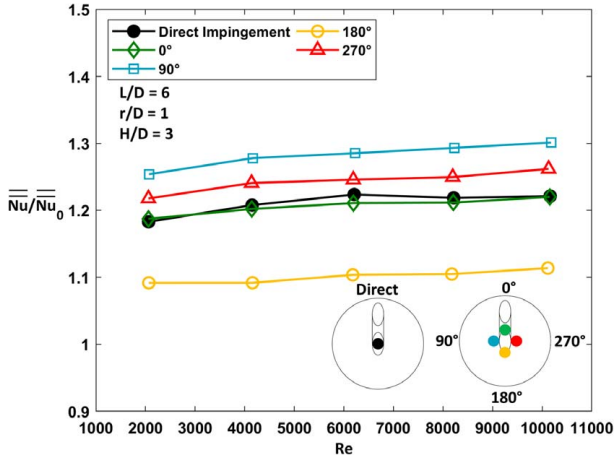

Fig. 8 Nusselt number augmentation relative to the no impingement case for *L/D* = 6

In addition to the augmentation of the convective heat transfer that occurs resulting from the entry region of the effusion hole relative to a fully developed pipe flow, there is also significant augmentation for the impingement cases relative to that of no impingement. Figures 7 and 8 directly show the heat transfer augmentation for the jet impingement relative to the no impingement case for both the long and short effusion holes for the circumferentially varying jet locations. The augmentation results indicate that there is no dependence on the Reynolds number with essentially a constant value for a given geometry. For each impingement case, the augmentation is always higher for the shorter hole length at $L/D = 3$ relative to the longer hole length at $L/D = 6$.

In Figs. 7 and 8, the augmentation results for both the long and short effusion holes indicate that the highest Nusselt number augmentations occur when the impingement jet is positioned at the sides of the film-cooling holes, $\theta = 90$ deg and 270 deg even more so than when there is direct impingement, which is also shown in Figs. 5 and 6. It may be expected that, given these locations are symmetric, the same augmentation levels would result. For the short effusion hole, the same augmentation did occur for the $\theta = 90$ deg and 270 deg cases, but for the longer effusion hole, there was a slightly higher augmentation for the $\theta = 90$ deg case relative to the $\theta = 270$ deg case. This difference is attributed to the significant sensitivity of the flowfield at the entrance to the cooling hole.

The lowest Nusselt number augmentation for the impingement cases occur when the impingement is positioned most closely to the effusion hole upstream entrance location at $\theta = 180$ deg as shown in Figs. 7 and 8.

To further evaluate the differences in augmentation from varying the impingement positions shown in Figs. 7 and 8, local Nusselt numbers at the entrance of the effusion holes (10% along the length of the hole, $\ell/D = 0.3$ for the $L/D = 3$; and $\ell/D = 0.6$ for the $L/D = 6$) were plotted in Figs. 9 and 10 for $\mathrm{Re} = 8000$. As would be expected in Figs. 9 and 10, the local heat transfer coefficients are relatively symmetric for the impingement locations of $\theta = 0$ deg and 180 deg with only slight anomalies for the $\theta = 0$ deg in Fig. 9 for the short L/D hole, which is attributed to the sensitivity due to the separation region.

For both L/D geometries in Figs. 9 and 10, the general spread of the local convective heat transfer coefficients when plotted was similar. At the same case for the $\phi = 0$ deg position, a substantial drop in the Nusselt number is observed regardless of L/D. This drop is indicative of the flow separation region as described in Kohli and Thole's [7] CFD analyses, which is caused by the turning angle of the fluid into the hole. It is important to note, however, that not exactly the same values occurred, which is related to the fact that in both cases these measurements were

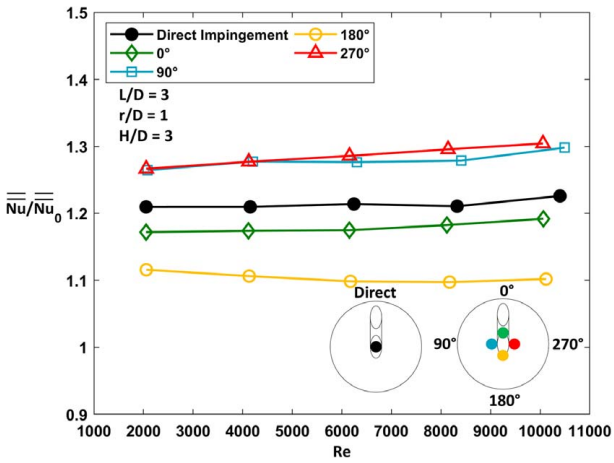

Fig. 7 Nusselt number augmentation relative to the no impingement case for *L/D* = 3

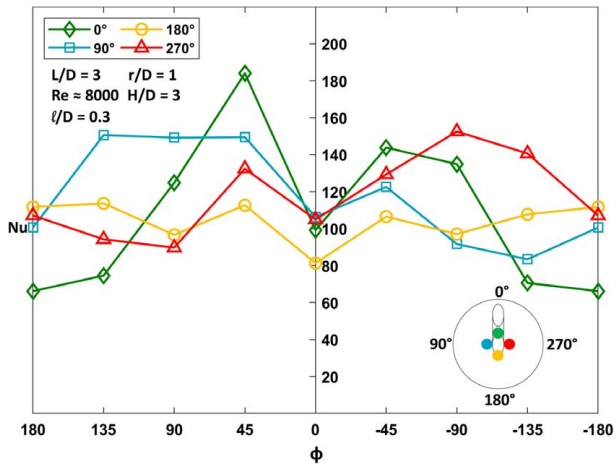

Fig. 9 Local Nusselt numbers around the effusion hole entrance at the *l/D* = 0.3 position for the *L/D* = 3 effusion hole

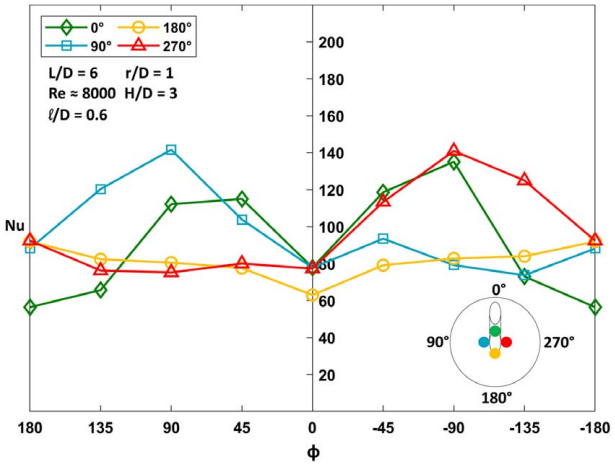

Fig. 10 Local Nusselt numbers around the effusion hole entrance at the *l*/D = 0.6 position for the *L*/*D* = 6 effusion hole

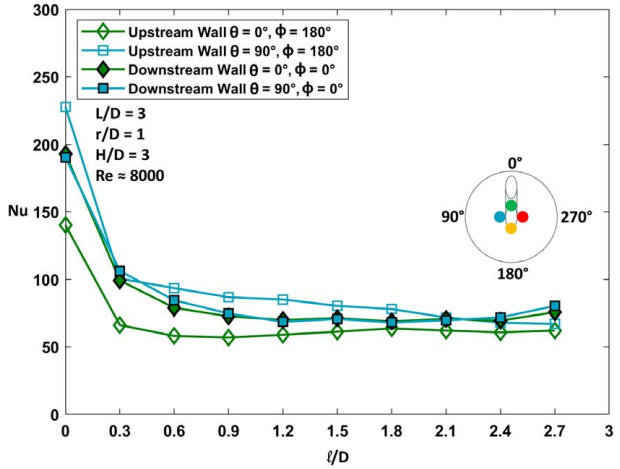

Fig. 11 Local Nusselt numbers along the upstream and downstream lengths of the effusion holes contrasting two different impingement locations for *L*/*D* = 3, *r*/*D* = 1, and *H*/*D* = 3

taken at 10% of the total length of the hole, which is effectively a larger downstream distance for the longer cooling hole case of $L/D = 6$ relative to the shorter cooling hole case of $L/D = 3$. When comparing $L/D = 3$ to $L/D = 6$ at $\phi = 0$ deg, the local heat transfer coefficients are nominally 30% higher for the $L/D = 3$ case, further illustrating the importance of the entrance region effects on heat transfer from the effusion holes.

As expected, Figs. 9 and 10 show that there is an increase in the local heat transfer coefficients for the $\theta = 90$ deg and 270 deg cases on the side of the effusion hole where the impingement took place. These local increases translate to higher overall averages of the heat transfer augmentation for the $\theta = 90$ deg and 270 deg cases as shown in Figs. 7 and 8. The reason for these increased heat transfer coefficients, more so than other impingement locations, is because of the differing entrance flow conditions. Kohli and Thole's [7] study showed that, depending on the feed location of a film-cooling hole, it is possible to alter the flow separation angle, which is present in the case of most film-cooling type flows, and even induce a swirl.

The hypothesis of an induced swirl for the $\theta = 90$ deg and 270 deg impingement cases at the hole entrance is supported by contrasting the data given in Fig. 11, which shows the streamwise distribution of the local heat transfer coefficients on both the upstream and downstream walls of the effusion holes for the $\theta = 0$ deg and 90 deg tests for the short $L/D = 3$ hole. Referring back to Fig. 2, it is important to note that for the $\theta = 0$ deg, the impinging fluid is targeting the upstream wall of the hole entrance. For the impingement fluid to enter the effusion hole, a large flow turning angle is required, which induces a separation region on the upstream wall. It would be expected that for the $\theta = 0$ deg case, the large separation along the upstream wall of the effusion hole would result in lower convective heat transfer coefficients, which, in fact, is shown in Fig. 11. In contrast, for the $\theta = 90$ deg case, the upstream wall has significantly higher local heat transfer coefficients along the wall. In both the $\theta = 0$ deg and 90 deg cases, the local heat transfer coefficients along the downstream wall are nominally the same along the length of the pipe.

Effect of Impingement Radial Spacing

To determine the sensitivity of the radial location of the impingement jets, the impingement hole positioned at $r/D = 3$ was contrasted to that of $r/D = 1$, leaving the jet-to-target spacing constant at $H/D = 3$ for both effusion hole lengths. In Figs. 12 and 13, the area-averaged Nusselt numbers for the increased radial position are compared to the close radial position. Three angular θ locations, $\theta = 0$ deg, 90 deg, and 180 deg, are shown in this section, as the $\theta = 90$ deg and 270 deg impingement locations have similar results.

It is expected that for the varying radial spacing of the impingement jet in Figs. 12 and 13, there is a substantial decrease in the heat transfer for the larger radial impingement placement ($r/D = 3$) for both the $\theta = 0$ deg and 90 deg cases relative to the close spacing, regardless of the Reynolds number. This decrease is seen for both $L/D = 3$ and $L/D = 6$. In contrast, for the $\theta = 180$ deg impingement location, higher heat transfer occurs for the larger radial spacing ($r/D = 3$) relative to the close spacing ($r/D = 1$) for both effusion hole lengths. This effect is due to a separation region created by the farther radial spacing.

As shown in Fig. 14, for the close radial spacing, the upstream wall has an increased Nusselt number along $\ell/D < 1.5$ when compared to the far radial spacing. However, at $\ell/D \geq 1.5$, the upstream wall heat transfer collapses onto the same line for both r/D impingement positions. In addition, the downstream wall Nusselt number of the close radial spacing test is lower throughout the entire length of the effusion hole, while the downstream wall of the far radial spacing Nusselt number is on par with its respective upstream wall results past $\ell/D = 0$. At the close radial spacing for the $\theta = 180$ deg case, the upstream and downstream wall results are indicative of a direct impingement-like effect where the flow is attached to the upstream wall along the majority of the effusion hole length, leading to the large difference in the Nusselt number for both walls. For the far radial impingement at $\theta = 180$ deg, the flow was more

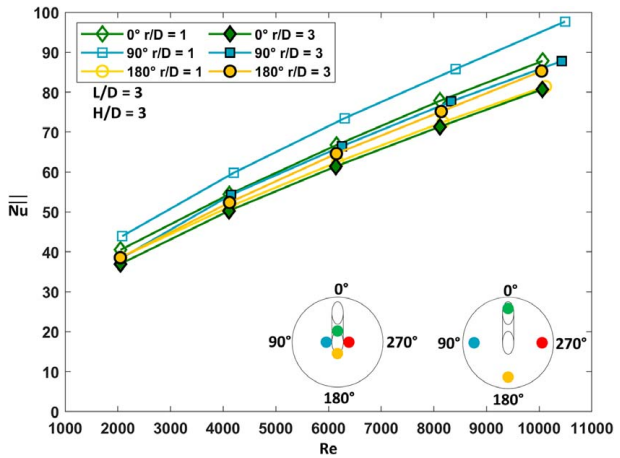

Fig. 12 Area-averaged Nusselt number with changing *r*/*D* and θ for the *L*/*D* = 3 effusion hole

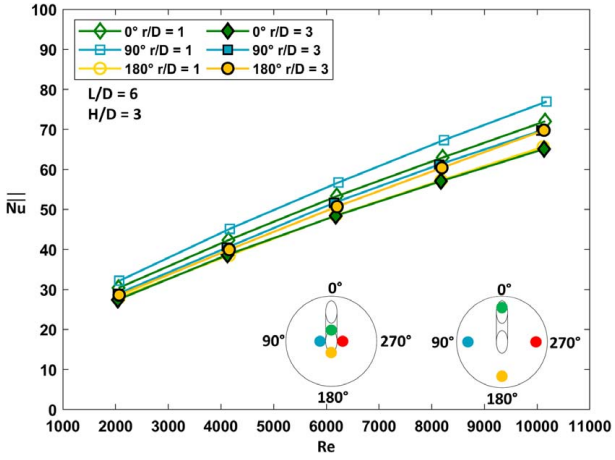

Fig. 13 Area-averaged Nusselt number with changing *r/D* and θ for the *L/D* = 6 effusion hole

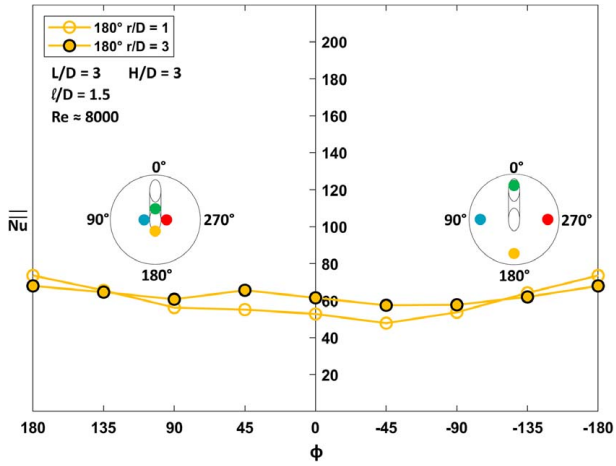

Fig. 15 Local Nusselt numbers around the effusion hole at the midpoint, *l/D* = 1.5, position for the *L/D* = 3 effusion hole

like a co-flowing crossflow as shown in the study by Kohli and Thole [7]. This crossflow initially had less cooling effectiveness at the entrance, but since the flow was more like a fully developed flow along the length of the hole rather than just the upstream wall as in the $r/D = 1$ position, it had better cumulative heat transfer. This effect of higher heat transfer at downstream ℓ/D locations is also supported by the circumferential local Nusselt numbers at $\ell/D = 1.5$ as shown in Fig. 15. In Fig. 15 for the close radial spacing, the upstream wall has higher heat transfer that decreases by a significant amount along the downstream wall. Conversely, the far radial spacing at $\ell/D = 1.5$ has an almost constant convection effect around the circumference of the effusion hole that is on par with the upstream wall values seen in the $r/D = 1$ case.

The heat transfer augmentation of the $r/D = 1$ locations over the $r/D = 3$ locations is displayed in Fig. 16. Since the area-averaged Nusselt number augmentation is generally the same between effusion hole lengths, as show in the previous figures, Fig. 16 is not replicated for the long effusion hole. For both the $\theta = 90$ deg and 0 deg cases, the close radial spacing of the impingement holes leads to roughly a 10% increase in the area-averaged Nusselt number across all Reynolds numbers when compared to the far radial spacing. The upstream impingement location, $\theta = 0$ deg, is not affected as much by the increase in radial spacing, and there is, on average, a 3% decrease in the area-averaged Nusselt number between the $r/D = 1$ impingement site and the $r/D = 3$ impingement site.

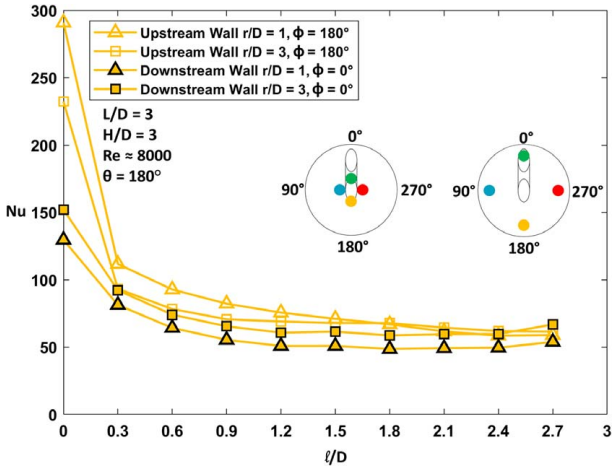

Fig. 14 Local Nusselt number along the upstream and downstream walls contrasting two *r/D* values at θ = 180 deg

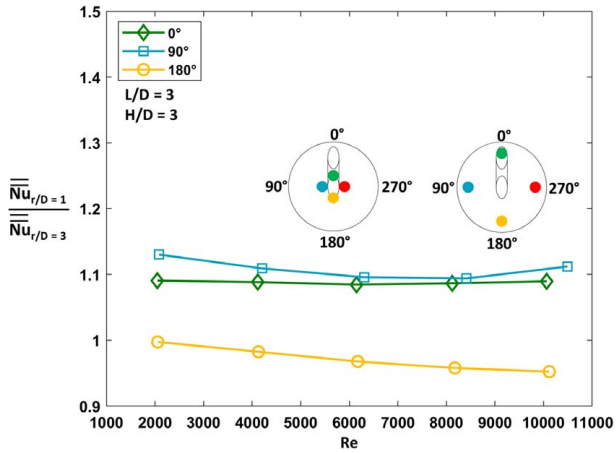

Fig. 16 Average Nusselt number augmentation of the close radial spacing compared to the far radial spacing for the *L/D* = 3 and *H/D* = 3 geometry

Effect of Jet-to-Target Spacing

The impingement jet-to-target spacing was varied to determine the effects on the sensitivity of the convective heat transfer. For these experiments, the closest radial spacing was used at $r/D = 1$ for both short and long hole lengths. The data for the two hole lengths are shown in Figs. 17 and 18 to compare the area-averaged Nusselt numbers for the close impingement location, $H/D = 3$, to the far impingement location, $H/D = 6$.

The results in Figs. 17 and 18 show that there is little sensitivity in the area-averaged Nusselt number when changing the jet-to-target distance except for the $\theta = 90$ deg case, which shows a higher convective heat transfer coefficient for the closer target spacing of $H/D = 3$ relative to $H/D = 6$. Given that all the results presented in this article up to this point consistently point to the turning of the impingement flow into the cooling hole having a large impact on the effusion hole convection, it is expected that the data shown in Figs. 17 and 18 are consistent. By placing the impingement hole at $\theta = 90$ deg, increases in convective heat transfer can be gained; however, as the impingement jet is moved further from the effusion hole, this benefit decreases resulting in lower convective heat transfer for the $\theta = 90$ deg case with larger jet-to-target distance of $H/D = 6$. In Fig. 19, it is shown that there is little to no change in heat transfer augmentation of the $H/D = 3$ location versus the $H/D = 6$ location for the $\theta = 0$ deg and 180 deg angular

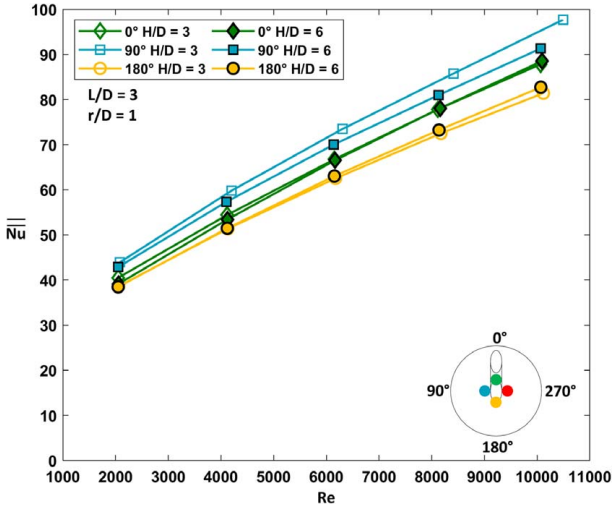

Fig. 17 Total area-averaged Nusselt number with varying jet-to-target spacing for r/D = 1 and L/D = 3

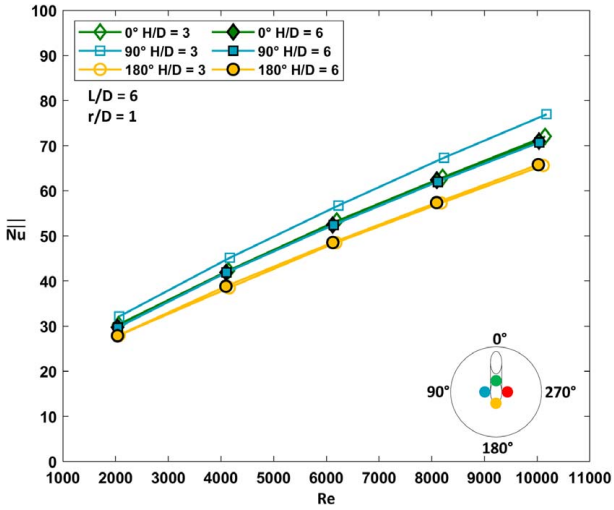

Fig. 18 Total area-averaged Nusselt number with varying jet-to-target spacing for *r/D* = 1 and *L/D* = 6

impingement positions, although the θ = 90 deg site had a 3.5% decrease on average when increasing the spacing.

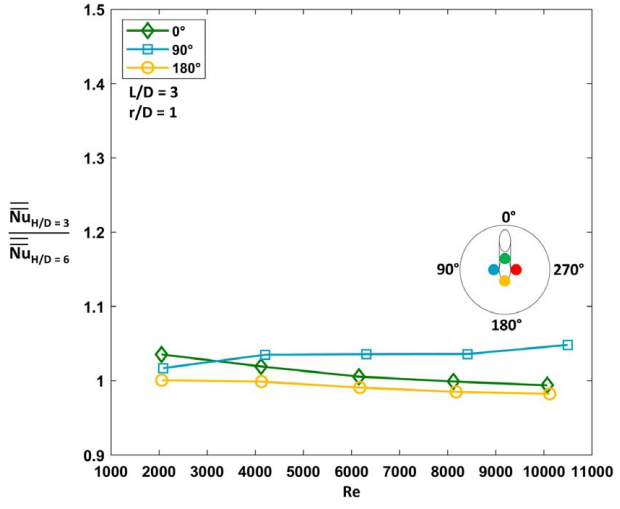

Fig. 19 Average Nusselt number augmentation of the close impingement jet-to-effusion hole spacing compared to the large spacing for a radial spacing for the *r/D* = 1 and *L/D* = 3 geometry

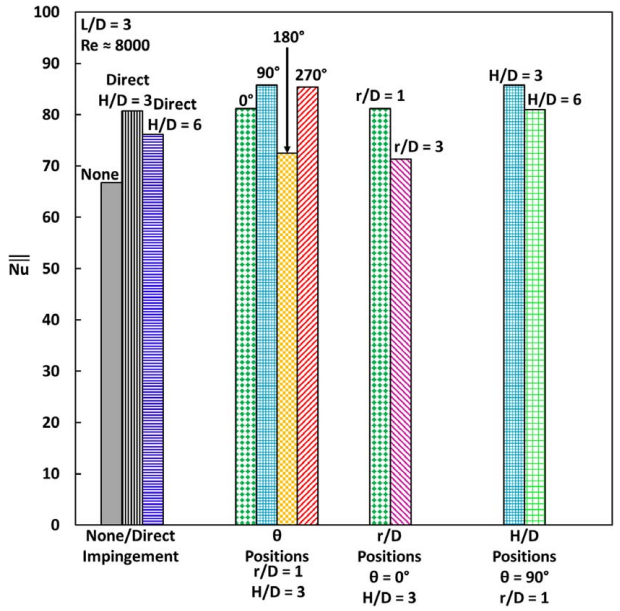

Fig. 20 Total area-averaged Nusselt number summary for *L/D* = 3

Summary

Overall, impingement positioning can have a large effect on the convective heat transfer inside of effusion holes. Figures 20 and 21 show a complete summary of the effects of the impingement position on the area-averaged Nusselt number as put forth in this study. The effusion hole length did not strongly affect the trends seen between impingement cases although the shorter *L/D* = 3 effusion hole had higher Nusselt numbers given the stronger influence of the entrance region. For all the cases tested, Figs. 20 and 21 show that higher convective heat transfer within the effusion hole occurred when there was impingement relative to no impingement case by 10%–30%.

The highest effusion hole heat transfer came from cases with close radial spacing, close impingement jet-to-effusion plate distance when the impingement jet was positioned at either the θ = 90 deg and 270 deg locations. As mentioned earlier, these cases create a swirl at the entrance region overcoming any jet separation effects.

Increasing radial spacing, *r/D*, led to decreases in convection for most cases as shown in Figs. 20 and 21, except for θ = 180 as previously explained. Finally, increasing jet-to-target spacing, *H/D*, had little effect on the area-averaged Nusselt number except in the direct impingement case and the θ = 90 deg case shown in the figures, where it slightly decreased.

Conclusions

The cooling of combustor liners are typically done through the use of a double-wall geometry containing both an impingement jet that supplies an effusion hole. These designs heavily depend on the convective nature of the effusion holes to contribute to the overall liner cooling.

An experiment was constructed to contain a scaled-up, double-wall containing a single impingement jet feeding a single effusion

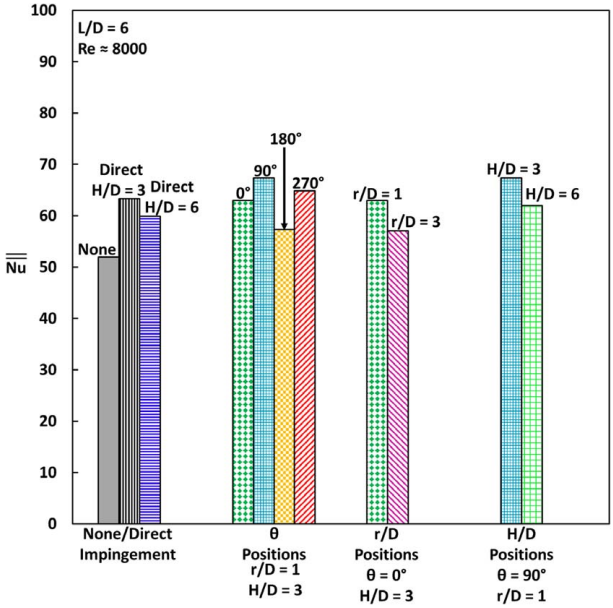

Fig. 21 Total area-averaged Nusselt number summary for $L/D = 6$

hole to better understand the convective the influences on the effusion hole. The impingement hole was varied in angular and circumferential positions relative to the effusion hole for two different effusion hole lengths. In addition, the impingement jet-to-effusion hole positioning was changed. A constant heat flux was imposed on the effusion hole inner surface to evaluate the convective heat transfer at various Reynolds numbers.

All impingement cases were found to be much higher than the fully developed pipe flow correlation as expected due to the short hole lengths and the entry region effects. The experiments showed that impingement contributes to higher convective heat transfer by as much as 10%–30% depending on the impingement placement. At a close radial spacing and close jet-to-target spacing, the highest convective heat transfer occurred for the jet impingement occurring at the sides of the effusion hole. The increased augmentation seen for the side impingement locations was due to an induced swirl seen in the previous studies, which increases the heat transfer along the length of the effusion hole and reduces the separation region at the hole entrance. This increase was seen in the local Nusselt number measurements at the entrance and on the upstream and downstream walls along the length of the hole.

The data presented that there was little effect on the convective heat transfer within the effusion hole with differing impingement jet-to-effusion hole spacing. This particular result enforces the finding that the dominating effect on the effusion hole convection has to do with how the coolant enters into the effusion hole. Also, while the effusion hole lengths tested affected the Nusselt number values, they did not have a large effect on the general trends between impingement cases.

In summary, it was found that the impingement location can have a large effect on the heat transfer inside effusion cooling holes. This study adds to the body of knowledge for impingement and effusion cooling in double-wall combustor liners. The results displayed can assist in understanding and optimizing the impingement hole placement for improved in-hole heat transfer, which is an important parameter to cooling combustor liners.

Acknowledgment

The authors would like to thank Pratt & Whitney for the technical and financial support given for this research.

Conflict of Interest

There are no conflicts of interest.

Data Availability Statement

The datasets generated and supporting the findings of this article are obtainable from the corresponding author upon reasonable request. The authors attest that all data for this study are included in the paper.

Nomenclature

h = local heat transfer coefficient
ℓ = distance along effusion hole
r = radial distance from impingement plate center
A = local surface area
D = impingement and effusion hole diameter
H = impingement jet-to-effusion plate spacing
L = effusion hole length
$\overline{\overline{h}}$ = area-averaged heat transfer coefficient
$\dot{m}$ = mass flowrate
q'' = heat flux
$\overline{\overline{Nu}}$ = area-averaged Nusselt number ($\overline{\overline{h}}D/k_{air}$)
$\overline{\overline{Nu_0}}$ = $\overline{\overline{Nu}}$, no impingement case
k_{air} = thermal conductivity of air
t_e = effusion plate thickness
t_i = impingement plate thickness
A_{total} = total surface area
T_{air} = local mean air temperature
T_w = local effusion surface temperature
Nu = Nusselt number (hD/k_{air})
Re = Reynolds number ($\dot{m}/\mu^{-1}/(\pi/4)/D$)

Greek Symbols

α = effusion inclination angle
θ = impingement circumferential location angle
μ = dynamic viscosity
ϕ = effusion circumferential location angle

References

[1] Scrittore, J. J., Thole, K. A., and Burd, S. W., 2005, "Experimental Characterization of Film-Cooling Effectiveness Near Combustor Dilution Holes," ASME Turbo Expo 2005: Power for Land, Sea, and Air, Reno, NV, June 6–9, Paper No. GT2005-68704.
[2] Scrittore, J. J., Thole, K. A., and Burd, S. W., 2007, "Investigation of Velocity Profiles for Effusion Cooling of a Combustor Liner," ASME J. Turbomach., **129**(3), pp. 518–526.
[3] Shrager, A. C., Thole, K. A., and Mongillo, D., 2019, "Effects of Effusion Cooling Pattern Near the Dilution Hole for a Double-Walled Combustor Liner—Part 1: Overall Effectiveness Measurements," ASME J. Eng. Gas Turbines Power, **141**(1), p. 011022.
[4] Shrager, A. C., Thole, K. A., and Mongillo, D., 2019, "Effects of Effusion Cooling Pattern Near the Dilution Hole for a Double-Walled Combustor Liner—Part II: Overall Effectiveness Measurements," ASME J. Eng. Gas Turbines Power, **141**(1), p. 011023.
[5] Boelter, L. M. K., Young, G., and Iverson, H. W., 1948, "An Investigation of Aircraft Heaters XXVII—Distribution of Heat-Transfer Rate in the Entrance Section of a Circular Tube," NACA Technical Note No. 1451.
[6] Cho, H. H., Jabbari, M. Y., and Goldstein, R. J., 1997, "Experimental Mass (Heat) Transfer in and Near a Circular Hole in a Flat Plate," Int. J. Heat Mass Transfer., **140**(10), pp. 2431–2443.
[7] Kohli, A., and Thole, K. A., 1997, "A CFD Investigation on the Effect of Entrance Flow Conditions in Discrete Film Cooling Holes," 32nd National Heat Transfer Conference, Baltimore, MD, Aug. 8–12, Vol. 12, pp. 223–232.
[8] Martiny, M., Schulz, A., and Wittig, S., 1997, "Mathematical Model Describing the Coupled Heat Transfer in Effusion Cooled Combustor Walls," ASME 1997 International Gas Turbine and Aeroengine Congress and Exhibition, Orlando, FL, June 2–5, Paper No. 97-GT-329.

[9] Terrell, E. J., Mouzon, B. D., and Bogard, D. G., 2005, "Convective Heat Transfer Through Film Cooling Holes of a Gas Turbine Blade Leading Edge," ASME Turbo Expo 2005: Power for Land, Sea, and Air, Reno, NV, June 6–9, Paper No. GT2005-69003.
[10] Bryant, E. C., and Rutledge, J. L., 2019, "A Computational Technique to Evaluate the Relative Influence of Internal and External Cooling on Overall Effectiveness," ASME Turbo Expo 2019: Turbomachinery Technical Conference and Exposition, Paper No. GT2019-90999.
[11] Cho, H. H., and Goldstein, R. J., 1995, "Heat (Mass) Transfer and Film Cooling Effectiveness With Injection Through Discrete Holes: Part I—Within Holes and on the Back Surface," ASME J. Turbomach., **117**(3), pp. 440–450.
[12] Kline, S. J., and McClintock, F. A., 1953, "Describing the Uncertainties in Single Sample Experiments," Mech. Eng., **75**(1953), pp. 3–8.
[13] Gnielinski, V., 1976, "New Equations for Heat and Mass Transfer in Turbulent Pipe and Channel Flow," Int. Chem. Eng., **16**(2), pp. 359–368.